Journal of Materials Chemistry C

RSC Publishing

PAPER

View Article Online
View Journal | View Issue

Cite this: J. Mater. Chem. C, 2013, 1, 2224

Evaluation of propylene-, *meta*-, and *para*-linked triazine and *tert*-butyltriphenylamine as bipolar hosts for phosphorescent organic light-emitting diodes†

Qiang Wang,[a] Jason U. Wallace,[b] Thomas Y.-H. Lee,[a] Jane J. Ou,[a] Yu-Tang Tsai,[c] Yi-Hsiang Huang,[c] Chung-Chih Wu,[c] Lewis J. Rothberg[d] and Shaw H. Chen*[ae]

Received 8th November 2012
Accepted 27th January 2013

DOI: 10.1039/c3tc00588g

www.rsc.org/MaterialsC

Three representative bipolar hybrids – ***t*Bu-TPA-*p*-TRZ**, ***t*Bu-TPA-*m*-TRZ**, and ***t*Bu-TPA-$\mathscr{L}$-TRZ** with triplet energies, E_T = 2.5, 2.7 and 3.0 eV, respectively – were synthesized and characterized for a comprehensive evaluation of their potential as a host for phosphorescent organic light-emitting diodes (PhOLEDs) using red-emitting **Ir(piq)$_3$** as the dopant with an E_T value of 2.1 eV. Formation of charge transfer complexes, CTCs, was diagnosed by fluorescence bathochromism in increasingly polar solvents. Both intra- and inter-molecular charge transfer processes are invoked to explain CTC formation in all three hybrids. The ***p***-hybrid is by far the most susceptible to CTC formation both in solution and neat solid film, resulting in PhOLEDs with reduced external quantum efficiency, EQE, despite the best balance between charge fluxes across the emitting layer, EML, as revealed by the electron- and hole-only devices in addition to PhOLEDs containing a sensing layer. The highest EQE is achieved with the ***m***-hybrid thanks to the compromise between balanced charge fluxes and CTC formation. The $\mathscr{L}$-hybrid is the least prone to CTC formation while suffering charge flux imbalance to yield an EQE intermediate between those of the ***m***- and ***p***-hybrids. The least CTC formation involving the $\mathscr{L}$-hybrid is advantageous in accommodating the most singlets and triplets readily transferrable to both red and blue phosphors on account of its relatively high E_T value. Furthermore, the $\mathscr{L}$-hybrid offers the best morphological stability of the desired glassy EML, thus holding promise for the fabrication of superior PhOLEDs overall.

Introduction

Phosphorescent organic light-emitting diodes, PhOLEDs, have been intensively investigated because of their promise for solid-state lighting and flat panel displays.[1] The triplet emitter is preferably dispersed into a host at the molecular level to prevent concentration quenching.[2] Host materials used to prepare the emitting layer, EML, play a crucial role especially in blue PhOLEDs with adequate longevity, which have remained the main barrier to practical applications. To substantially improve device efficiency and lifetime simultaneously, it is imperative that excitons be evenly distributed through EML, and that the accumulation of charges and excitons at interfaces be prevented. Mixtures of electron- and hole-transport components have been widely employed to accomplish bipolar charge transport.[3] Alternatively, chemical hybrids offer tunable charge injection and transport with superior morphological properties while avoiding phase separation and crystallization.[4] To attain sufficiently high triplet energies, E_T, so that the hosts are amenable to blue phosphors, π-conjugation between the electron- and hole-transport moieties should be minimized or prevented altogether through a large torsion angle,[5] *meta*-substitution,[6] or insertion of an sp^3-hybridized C or Si atoms.[7,8] The coexistence of electron- and hole-transport moieties, however, may lead to intra- or intermolecular charge transfer as widely reported in bipolar hosts.[6,9] The formation of charge transfer complexes, CTCs, entails an appreciable differences in HOMO and LUMO energies, Δ(HOMO) and Δ(LUMO) between the donor and acceptor.[10] Adachi *et al.*[11] reported CTC

[a]Department of Chemical Engineering, University of Rochester, Rochester, NY 14627, USA. E-mail: shch@lle.rochester.edu
[b]Department of Mathematics and Natural Sciences, D'Youville College, Buffalo, NY 14201, USA
[c]Department of Electrical Engineering, Graduate Institute of Electronics Engineering, and Graduate Institute of Photonics and Optoelectronics, National Taiwan University, Taipei 10617, Taiwan, Republic of China
[d]Department of Chemistry, University of Rochester, Rochester, NY 14627, USA
[e]Laboratory for Laser Energetics, University of Rochester, Rochester, NY 14623, USA

† Electronic supplementary information (ESI) available: Reaction scheme and experimental procedures for the synthesis and purification with characterization data for bipolar hybrids. Proton-NMR spectra in $CDCl_3$; cyclic voltammetric scans of ***t*Bu-TPA**, **TRZ**, ***t*Bu-TPA-*p*-TRZ**, ***t*Bu-TPA-*m*-TRZ**, and ***t*Bu-TPA-$\mathscr{L}$-TRZ** at 10^{-3} M in acetonitrile : toluene (1 : 1 by volume) with 0.1 M tetrabutylammonium tetrafluoroborate as the supporting electrolyte; fluorescence spectra of ***t*Bu-TPA-*m*-TRZ** and ***t*Bu-TPA-$\mathscr{L}$-TRZ** in toluene, chloroform, and DMF with photoexcitation at 277 nm; and the DSC heating and cooling scans of ***t*Bu-TPA-*p*-TRZ**, ***t*Bu-TPA-*m*-TRZ**, and ***t*Bu-TPA-$\mathscr{L}$-TRZ** without and with **Ir(piq)$_3$** at 8 wt%, all pretreated to eliminate thermal history. See DOI: 10.1039/c3tc00588g

formation with a Δ(HOMO) value ≥0.4 eV in mixtures of Alq_3 with various hole-transport materials, but no quantitative correlation with the difference between LUMO levels has been reported. Therefore, the CTC formation has remained unpredictable *a priori*. Although a number of bipolar hosts have been shown to afford high external quantum efficiency,[4] EQE, CTC formation is a potential cause for diminished device efficiency and spectral impurity.[12] It is important that CTC formation be probed in bipolar hosts to figure out how to avoid it through molecular design. In the present study, ***t*Bu-TPA-*p*-TRZ**, ***t*Bu-TPA-*m*-TRZ**, and ***t*Bu-TPA-*ℒ*-TRZ** representing a broad spectrum of prospective linked host materials were synthesized by covalently attaching triazine[13,14] to triphenylamine[15,16] as typical charge-transport moieties in three different ways. The HOMO/LUMO levels, E_Ts, propensity for CTC formation, and morphological stability against crystallization of an EML containing **Ir(piq)$_3$** with a lower E_T than the three hybrids are characterized to increase their potential as prospective hosts. The implications of the outcome of this study on blue-emitting PhOLEDs will also be highlighted.

Results and discussion

Depicted in Chart 1 are three prototypical bipolar hybrids, ***t*Bu-TPA-*p*-TRZ**, ***t*Bu-TPA-*m*-TRZ** and ***t*Bu-TPA-*ℒ*-TRZ**, with *para*- and *meta*-linkages and a propylene spacer. The *tert*-butyl groups on the **TPA** moiety are intended to overcome electrochemical instability by blocking the active *para*-sites on phenyl rings.[17] It has been reported that **TRZ** exhibits reversible reduction in its cyclic voltammetry, CV, scan without protection.[18] Indeed, the three bipolar hybrids exhibited reversible oxidation and reduction scans in dilute solution (Fig. S1†) for the measurement of half-wave potentials used to calculate HOMO and LUMO levels in neat solid films.

The high-energy absorption bands from 250 to 350 nm in dilute chloroform solution shown in Fig. 1a for ***p*-**, ***m*-**, and *ℒ*-hybrids can be represented approximately by the sum of ***t*Bu-TPA** and **TRZ** absorption spectra. In addition, the ***p*-**hybrid presents a distinct absorption peak at 400 nm that can be assigned as photo-induced intramolecular CTC formation made possible by some degree of π-conjugation through the biphenyl core, which is substantially suppressed in the ***m*-**hybrid and absent in the *ℒ*-hybrid largely consistent with the calculated frontier molecular orbitals shown in Fig. 2. With excitation at 277 nm, fluorescence of both ***t*Bu-TPA** and **TRZ** as independent chemical entities in chloroform at 10^{-5} M was below our detection sensitivity from 300 to 800 nm. Photoexciting each of the three hybrids in chloroform at the same concentration results in fluorescence at 535 nm, as shown in Fig. 1b and S2.† The fluorescence shifts strongly according to solvent polarity, from the blue in toluene and to the red in DMF, confirming our interpretation of CTC formation.[19,20] The relative intensities shown in Fig. 1b and c are consistent with intermolecular charge transfer being promoted by tighter molecular packing in neat solid film than in dilute solution. The observed fluorescence enhancement in neat solid film follows the sequence *ℒ*- > ***m*-** > ***p*-**hybrids, reflecting the increasing intermolecular over intramolecular CTC formation on the part of the *ℒ*-hybrid followed by the ***m*-**hybrid compared to the ***p*-**hybrid.

The intramolecular CTC formation in the *ℒ*-hybrid can be rationalized with molecular folding enabled by the flexible propylene spacer[21] without resorting to π-conjugation through a biphenyl core in the ground state (Fig. 2) and hence the absence of absorption at 400 nm unlike in the ***p*-**hybrid for which π-conjugation through the biphenyl core is visualized. While not captured by the calculated frontier molecular orbitals, there must be a finite extent of π-conjugation through the ***m*-**hybrid in the absence of molecular folding to support an intramolecular CT process while remaining insufficient to induce the 400 nm absorption peak. The PLQYs of 100 nm thick neat films of ***p*-**, ***m*-**, and *ℒ*-hybrids were characterized in an integrating sphere as 0.54, 0.43, and 0.20 with absorbances of 0.30, 0.37, and 0.39, respectively, at the 325 nm line of a He–Cd laser. The measured PLQYs are qualitatively consistent with the relative integrated fluorescence intensities in Fig. 1c. Overall, the extent of CTC formation is by far the most prominent in the ***p*-**hybrid, and the least in the *ℒ*-hybrid.

That the three hybrids have the same fluorescence peak wavelengths in neat solid films and in the various solvents could be the consequence of the same HOMO–LUMO gaps in a given medium,[22] as expected of the observed HOMO and LUMO levels presented in Table 1. To evaluate the prospects of the three hybrids as hosts in phosphorescent OLEDs, E_T values were characterized using phosphorescence spectroscopy in dichloromethane at 77 K (Fig. 3). A relatively long 10 ms delay between pulsed excitation and collection of emission spectra managed to minimize the contamination of hybrids' phosphorescence by CTC fluorescence in dichloromethane compared to toluene and chloroform (Fig. 1b). The challenge confronting the identification of relatively inconspicuous peaks for a determination of E_T values using phosphorescence spectra is well recognized.[23]

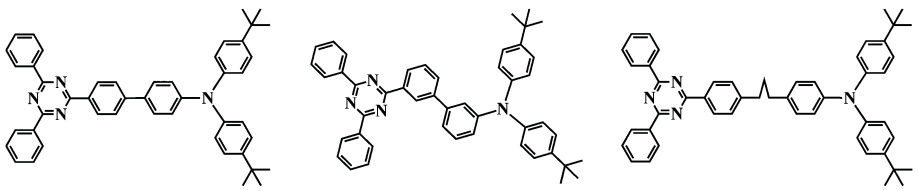

***t*Bu-TPA-*p*-TRZ**
G 132 °C, 192 °C *K* 282 °C *I*

***t*Bu-TPA-*m*-TRZ**
G 99 °C *I*

***t*Bu-TPA-*ℒ*-TRZ**
G 85 °C *I*

Chart 1 Molecular structures of hybrid compounds with their thermal transition temperatures determined by DSC second heating scans. Symbols: *G*, glassy; *K*, crystalline; *I*, isotropic.

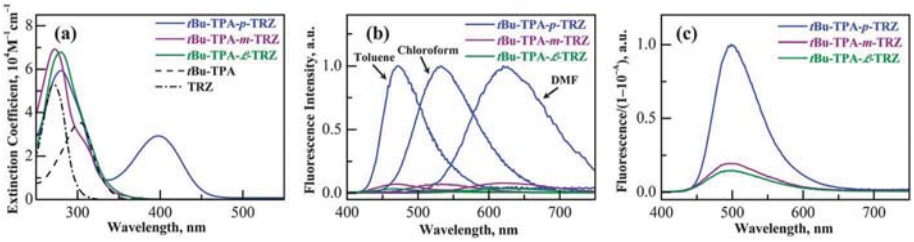

Fig. 1 Absorption spectra at 20 °C of (a) ***t*Bu-TPA**, **TRZ**, ***t*Bu-TPA-*p*-TRZ**, ***t*Bu-TPA-*m*-TRZ**, and ***t*Bu-TPA-ℒ-TRZ** in chloroform at 8.3×10^{-6} M; nearly identical absorption spectra were obtained for neat solid films of the three hybrids. Fluorescence spectra at 20 °C of (b) ***t*Bu-TPA-*p*-TRZ**, ***t*Bu-TPA-*m*-TRZ**, and ***t*Bu-TPA-ℒ-TRZ** in toluene, chloroform and *N*,*N*-dimethylformamide at 8.3×10^{-6} M with photoexcitation at 277 nm characterized by a peak-intensity ratio averaged over three solvents at 25 : 2 : 1 for ***p*- : *m*- : ℒ-**hybrid, see Fig. S2† for the enlarged spectra of the ***m*-** and **ℒ**-hybrids; and (c) ***t*Bu-TPA-*p*-TRZ** (95 nm), ***t*Bu-TPA-*m*-TRZ** (97 nm), and ***t*Bu-TPA-ℒ-TRZ** (94 nm) vacuum sublimed on fused silica substrates receiving the same incident excitation at 281 nm with fluorescence spectra normalized by 1 to 10^{-A}, where A is the absorbance of photoexcitation at 281 nm.

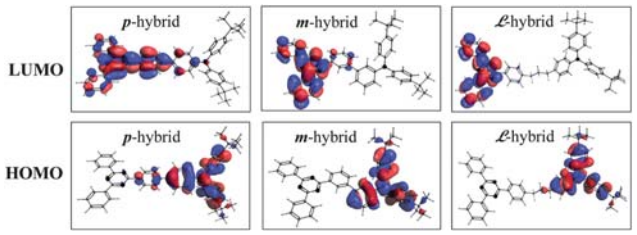

Fig. 2 Frontier molecular orbitals, *i.e.* HOMO and LUMO, calculated using the Gaussian 09 software package. In particular, molecular geometries were optimized with B3LYP/6-31G(d), and LUMO and HOMO molecular orbitals were calculated with t-HCTHhyb/6-311++G(d,p), revealing the limited π-conjugation through the twisted biphenyl core in the ***p*-**hybrid, but little or none in the ***m*-** and **ℒ**-hybrids. The black dots represent nitrogen atom where possible to avoid confusion with frontier molecular orbitals.

The measured E_T values are included in Table 1, which represent the electronic transition from the first triplet state, $T_1(\nu = 0)$, to the ground state, $S_0(\nu = 0)$, where $\nu = 0$ denotes the vibrational ground state. In its $T_1(\nu = 0)$ state, the biphenyl core has been reported to have a vanishing torsion angle[24] in contrast to ~40° in its $S_0(\nu = 0)$ state.[25] That the difference in the extents of π-conjugation through the biphenyl core in the $T_1(\nu = 0)$ state is more pronounced than in the $S_0(\nu = 0)$ state is borne out by the relative E_T values, ***p*- < *m*- < ℒ-**hybrids. Compared to their $S_0(\nu = 0)$ states, the $T_1(\nu = 0)$ state of the ***p*-**hybrid is resonance-stabilized to a greater extent than that of the ***m*-**hybrid. The absence of π-conjugation through the biphenyl core in both the $T_1(\nu = 0)$ and $S_0(\nu = 0)$ states enables the **ℒ**-hybrid to retain as its E_T the lower value of two contributed by independent **TPA** and **TRZ** moieties at 3.1 and 3.0 eV.[7,26] The E_T values of the ***p*-** and ***m*-**hybrids (2.5 and 2.7 eV, respectively) are inadequate for hosting blue phosphors, *e.g.* **FIrpic** (E_T = 2.6 eV), to deliver efficient PhOLEDs. The oft-quoted relationship, absorption edge = HOMO − LUMO, is obeyed by the ***p*-**hybrid with the 400 nm absorption peak representing the electronic transition from ***t*Bu-TPA**'s HOMO level to **TRZ**'s LUMO level, which is probed in the CV measurement. This electronic transition, however, is absent in the ***m*-** and **ℒ**-hybrids where the two moieties absorb light independently in the 250 to 350 nm spectral region. Within typical experimental errors, the HOMO and LUMO levels presented in Table 1 for the three hybrids are indistinguishable from those of the ***t*Bu-TPA** and **TRZ** precursors. Furthermore, the hybrids' HOMO/LUMO values are not sufficiently sensitive to the limited resonance stabilization in the ***p*-**hybrid over those of the ***m*-** and **ℒ**-hybrids as a result of the ~40° torsion angle within the biphenyl core in their $S_0(\nu = 0)$ states involved in the characterization of energy levels.

Based on the energy levels reported in Table 1, the three hybrids and their precursors share essentially the same HOMO and LUMO values for the construction of energy diagrams shown in Fig. 4. Inspired by Weller's early work on fluorescence from CTC between diethylaniline and anthracene in toluene,[29] fluorescence from the three hybrids in neat solid film and dilute solution can be rationalized in terms of both intramolecular and intermolecular charge transfer processes. Intramolecular charge transfer is depicted in Fig. 4a, where the electronic

Table 1 HOMO and LUMO levels in neat films characterized at 20 °C and triplet energies measured in dichloromethane at 77 K

Compound	$E_{1/2}$(oxd)[a] *vs.* Fc/Fc$^+$ (V)	$E_{1/2}$(red)[a] *vs.* Fc/Fc$^+$ (V)	HOMO[c] (eV)	LUMO[d] (eV)	E_T (eV)
***t*Bu-TPA**	0.42 ± 0.02	N.A.[b]	−5.2 ± 0.1	N.A.	3.1[e]
TRZ	N.A.[b]	−2.18 ± 0.02	N.A.	−2.2 ± 0.2	3.0[f]
***t*Bu-TPA-*p*-TRZ**	0.48 ± 0.01	−2.11 ± 0.02	−5.3 ± 0.1	−2.3 ± 0.2	2.5[g]
***t*Bu-TPA-*m*-TRZ**	0.49 ± 0.04	−2.13 ± 0.04	−5.3 ± 0.1	−2.3 ± 0.2	2.7[g]
***t*Bu-TPA-ℒ-TRZ**	0.40 ± 0.04	−2.19 ± 0.03	−5.2 ± 0.1	−2.2 ± 0.2	3.0[g]

[a] Half-wave potentials, $E_{1/2}$, relative to ferrocene/ferrocenium (Fc/Fc$^+$) with an oxidation potential at 0.51 V *vs.* Ag/AgCl, determined as the average of forward and reverse oxidation or reduction peaks. [b] Oxidation or reduction potential beyond the *CV* measurement range. [c] For neat solid films: HOMO = $-(1.4 \pm 0.1) \times qE_{1/2}$(oxd) $- (4.6 \pm 0.08)$ eV.[27] [d] For neat solid films: LUMO = $-(1.19 \pm 0.08) \times qE_{1/2}$(red) $- (4.78 \pm 0.17)$ eV;[28] the resulting HOMO and LUMO levels are equivalent to those measured by UPV and UV-vis absorption spectroscopy. [e] Phosphorescence in ethanol at 77 K.[26] [f] Phosphorescence in ethyl acetate at 77 K.[7] [g] E_T measured in dichloromethane at 77 K with a typical error of ±0.1 eV.

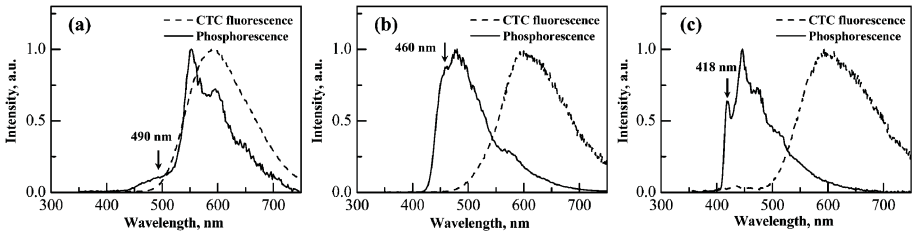

Fig. 3 Fluorescence from CTCs (20 °C, no time delay) and phosphorescence (77 K, 10 ms delay) of (a) ***t*Bu-TPA-*p*-TRZ** (excitation at 281 nm), (b) ***t*Bu-TPA-*m*-TRZ** (excitation at 273 nm), and (c) ***t*Bu-TPA-𝒮-TRZ** (excitation at 280 nm) in dichloromethane at 10^{-5} M. Triplet energies were estimated from the highest-energy vibronic sub-bands in the hybrids' phosphorescence spectra.

transition from the ***t*Bu-TPA**'s HOMO level to the **TRZ**'s LUMO level is responsible for absorption at 400 nm with subsequent vibrational relaxation within the same LUMO level, followed by radiative decay back to ***t*Bu-TPA**'s HOMO level as fluorescence at 500 nm. Both ***t*Bu-TPA** and **TRZ** moieties are shown in Fig. 4b to be independently excited at 281 nm followed by intramolecular charge transfer from ***t*Bu-TPA** to **TRZ** moieties, resulting in fluorescence at 500 nm. Fig. 4c describes intermolecular charge transfer to yield what is commonly referred to as exciplex, where (i) photoexcited electrons on ***t*Bu-TPA** are transferred to the lower-lying levels of **TRZ** in a neighboring molecule, and (ii) photoexcited electrons on **TRZ** are relaxed to the vibrational ground state within the same LUMO level, followed by fluorescence at 500 nm *via* another intermolecular process to ***t*Bu-TPA**'s HOMO level. In the case of ***p*-hybrid**, intramolecular charge transfer described in Fig. 4a makes a significant contribution to CTC formation in view of absorption at 400 nm. The other two mechanisms (Fig. 4b and c) may also proceed simultaneously to explain why nearly identical fluorescence peaks appear at 500 nm with excitation at 281 and 400 nm. The unique ability of the ***p*-hybrid** to undergo intramolecular charge transfer *via* direct absorption is understood in terms of relatively significant resonance stabilization of CTC depicted as part of Fig. 4a compared to both ***m***- and 𝒮-hybrids. Without absorption at 400 nm, the ***m***- and 𝒮-hybrids may proceed to CTC formation following the mechanisms described in Fig. 4b and/or c.

To evaluate PhOLED performance in relation to the extent of CTC formation, red-emitting **Ir(piq)$_3$** with an E_T of 2.1 eV (ref. 30) was doped in the three hybrids for the fabrication of devices: ITO/MoO_x(3 nm)/NPB(30 nm)/host:Ir(piq)$_3$(8 wt%, 20 nm)/BPhen(40 nm)/LiF(1 nm)/Al(100 nm); see Fig. 5a for its energy level diagram. Note that the E_T values of all three hybrids are higher than that of **Ir(piq)$_3$** to ensure energy transfer from the former to the latter but not *vice versa*. As shown in Fig. 5b, the highest EQE was achieved with the ***t*Bu-TPA-*m*-TRZ** containing device, while the ***t*Bu-TPA-*p*-TRZ** containing device yielded the lowest. The driving voltage, however, does not follow the same trend as EQE; see Fig. 5c. The ***t*Bu-TPA-𝒮-TRZ** containing device requires the highest driving voltage of the three hybrid hosts

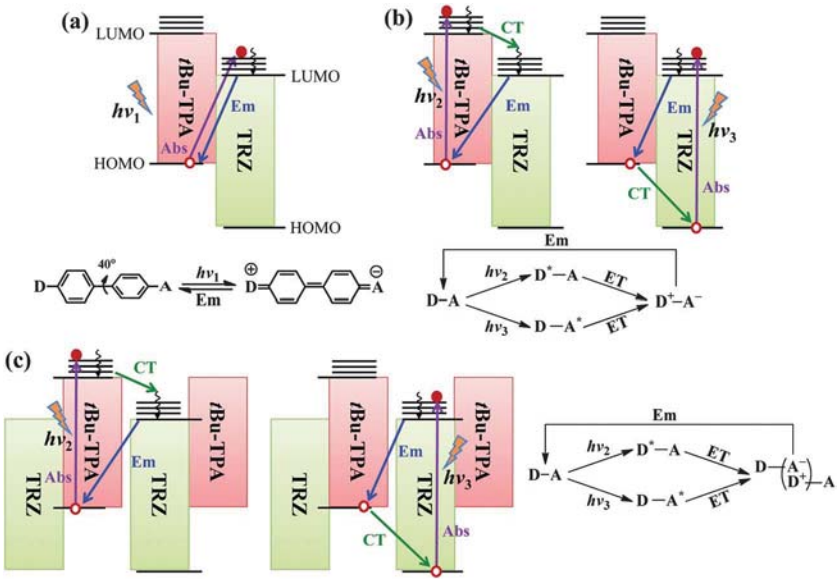

Fig. 4 Schematics of the charge transfer processes of ***t*Bu-TPA-*p*-TRZ**, ***t*Bu-TPA-*m*-TRZ** and ***t*Bu-TPA-𝒮-TRZ** in neat solid film and dilute solution: (a) intramolecular CTC responsible for absorption and fluorescence at 400 and 500 nm, respectively; (b) intramolecular CTC originating from independent light absorption by ***t*Bu-TPA** and **TRZ** moieties without absorption at 400 nm to yield fluorescence at 500 nm; and (c) intermolecular CTC originating from independent light absorption by ***t*Bu-TPA** and **TRZ** moieties without absorption at 400 nm to yield fluorescence at 500 nm. Symbols: Abs, absorption; Em, emission; D, donor (*i.e.* ***t*Bu-TPA**); A, acceptor (*i.e.* **TRZ**); CT, charge transfer; $h\nu_i$, photoexcitation.

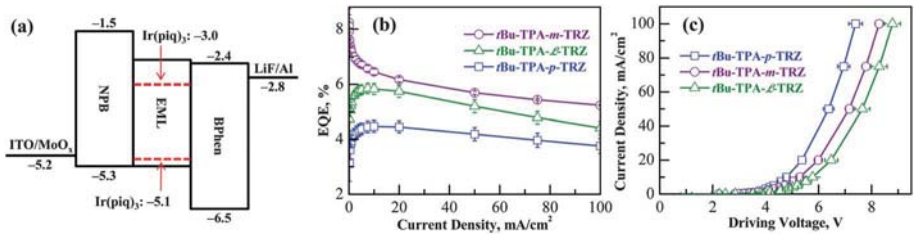

Fig. 5 (a) Energy diagram of the constructed PhOLEDs, in which the set of HOMO and LUMO values in eV presented in Table 1 are applied for the three hosts with the rest of values gleaned from the literature.[27,28,33–36] (b) EQE and (c) driving voltage as functions of current density for PhOLEDs with emitting layers comprising ***t*Bu-TPA-*p*-TRZ**, ***t*Bu-TPA-*m*-TRZ** and ***t*Bu-TPA-ℒ-TRZ** doped with 8 wt% **Ir(piq)$_3$**.

likely due to the poorest carrier mobility balance as demonstrated and explained below. With the three hybrid hosts having largely the same charge injection barriers (Table 1) incorporated in otherwise identical device architectures, the differences in EQE and driving voltage are accountable by the extents of CTC formation and unbalanced charge fluxes across the EML. In fact, charge recombination near the interface of the emitting layer with either the electron- or hole-transport layer can be detrimental to device efficiency and lifetime due to triplet–triplet annihilation[31] and triplet-polaron quenching[32] under high current densities pertaining to practical application.

The electroluminescence spectra shown in Fig. 6 indicate that the emission spectra of all three PhOLED devices are largely the same as the typical phosphorescence spectrum of **Ir(piq)$_3$** in dilute toluene solution.[30] It is arguable that the very weak CTC fluorescence peaks at about 500 nm in the electroluminescence spectra significantly underestimate the extents of CTC formation in the PhOLED. The energy level diagram shown in Fig. 5a suggests that direct recombination on the dopant molecules is favored, but some recombination on the host molecules must have also occurred to form CTCs therein. This conclusion is very important in that CTC formation can degrade PhOLED performance even when the HOMO and LUMO levels of the host are placed to avoid interfering with the dopant. It is insufficient for the host to have large gap and good energy level alignment, which is especially challenging to the design of hosts for blue phosphors. The CTC emission peaks from the hosts could have been further weakened by the very efficient Förster energy transfer from the emissive singlet CTCs to **Ir(piq)$_3$** at a 8 wt% doping level.[37,38] Nevertheless, the relative CTC emission intensities in the electroluminescence spectra do correlate with the extents of CTC formation inferred from PLQYs and the PL spectra in Fig. 1c of the neat host films. In addition, the endothermic Dexter energy transfer from the dopant to the host could form triplet CTCs[39] on the host molecules beyond the residual singlet CTC emission observed in Fig. 6a and b. These triplet CTCs on the hosts should be nonemissive[40] and quite possibly a source of quenching of dopant emission in the PhOLED.[11,41] Hence, the more prevalent the CTC formation is on the hosts, in the order ***p*- > *m*- > ℒ-hybrids** as indicated by Fig. 1c, the more significant the quenching should be in electroluminescence. All factors considered, the lowest EQE of the PhOLED comprising ***t*Bu-TPA-*p*-TRZ** (Fig. 5b) is attributable to the highest CTC fluorescence in its electroluminescence spectrum (Fig. 6a). In contrast, the lowest CTC fluorescence (Fig. 6c) and hence the most singlet and triplet formation following charge recombination on the ℒ-hybrid would result in energy transfer to the dopant, be it **Ir(piq)$_3$** or **FIrpic**, with an E_T value less than that of the host, an advantage to the PhOLEDs' EQEs over ***p*-** and ***m*-hybrids** as the hosts.

Relative charge transport capability and hence the deviation from balanced charge fluxes through the EML can be invoked to explain why ***t*Bu-TPA-*m*-TRZ** yields the highest EQE value followed by ***t*Bu-TPA-ℒ-TRZ**. Unipolar devices were fabricated to compare the charge transport capabilities of the three hybrids. The device structures of hole-only and electron-only devices are ITO/MoO_x(3 nm)/NPB(30 nm)/host(20 nm)/MoO_x(3 nm)/Al(100 nm) and ITO/Al(20 nm)/host(20 nm)/BPhen(40 nm)/LiF-(1 nm)/Al(100 nm), respectively. The three hybrids sustain identical hole fluxes (Fig. 7a), while the ***t*Bu-TPA-*p*-TRZ** containing device allows the highest electron flux (Fig. 7b) followed by ***t*Bu-TPA-*m*-TRZ** and then ***t*Bu-TPA-ℒ-TRZ** under the same driving voltage. That the three hybrids conduct holes more readily than electrons is demonstrated below using sensing layers.[42]

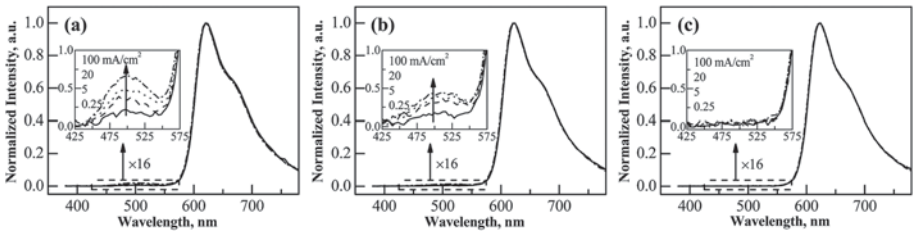

Fig. 6 Electroluminescence spectra of PhOLEDs with (a) ***t*Bu-TPA-*p*-TRZ**, (b) ***t*Bu-TPA-*m*-TRZ** and (c) ***t*Bu-TPA-ℒ-TRZ** as the hosts all doped at 8 wt% of **Ir(piq)$_3$** as functions of current densities. The CIE coordinates are (0.654, 0.333), (0.660, 0.330), and (0.670, 0.327) for the emission spectra shown in (a), (b), and (c), respectively. Insets: expanded views of emission spectra from 425 to 475 nm.

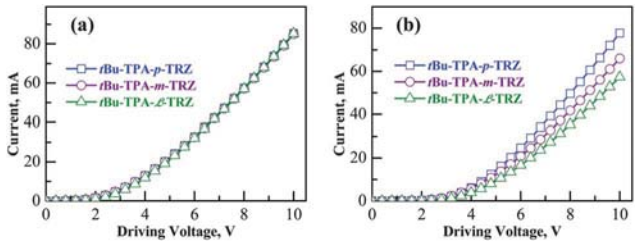

Fig. 7 Current as a function of driving voltage for (a) hole-only and (b) electron-only devices.

Depicted in Fig. 8a and b are the device structures in which NPB and BPhen are employed as the hole- and electron-transport layers, HTL and ETL, respectively, throughout this study. Additionally, a 3 nm-thick hybrid host doped with 8 wt% **Ir(piq)$_3$** is inserted as a sensing layer, one each at the HTL/EML and EML/ETL interfaces in two PhOLED devices. The ***t*Bu-TPA-*p*-TRZ** containing device with the sensing layer located at EML/ETL interface produced higher EQE than that with sensing layer at the HTL/EML interface (see Fig. 8c), suggesting that recombination occurs near the ETM/ETL interface and hence a higher hole flux than electron flux is encountered in this device despite the possibility of **Ir(piq)$_3$** assisting in electron transport. With the lower electron fluxes shown in Fig. 7b than ***t*Bu-TPA-*p*-TRZ**, the inferior balance of charge fluxes with ***t*Bu-TPA-*m*-TRZ** and ***t*Bu-TPA-𝒟-TRZ** as the hosts is expected. The experimental results summarized in Fig. 7 and 8 combine to imply that the ***t*Bu-TPA-*p*-TRZ** containing PhOLED possesses the best balance of charge fluxes across EML, while ***t*Bu-TPA-𝒟-TRZ** containing device the worst. Despite the best balance of charge fluxes, the device containing ***t*Bu-TPA-*p*-TRZ** produced the lowest EQE value because of the most loss of excitons to CTCs (see Fig. 6a). The better balance of charge fluxes in ***t*Bu-TPA-*m*-TRZ** containing device results in the higher EQE value than ***t*Bu-TPA-𝒟-TRZ** containing device despite the more pronounced CTC in the former (Fig. 6b *vs.* c). Although ***t*Bu-TPA-𝒟-TRZ** containing device did not manage to produce the highest EQE of the three, the flexible linkage is probably the most effective way to minimize loss of device efficiency and to attain high spectral purity by suppressing CTC formation. One can imagine numerous strategies, *e.g.* Meerheim *et al.*,[43] that remediate the charge flux imbalance in the 𝒟-hybrid host to benefit both EQE and device lifetime.

In addition to suppressing CTC formation, bipolar hybrids with a flexible linkage have the potential for strengthening the morphological stability of a glassy EML against phase separation and crystallization. The differential scanning calorimetric thermograms reveal that noncrystalline ***t*Bu-TPA-*m*-TRZ** and ***t*Bu-TPA-𝒟-TRZ** have glass transition temperatures, T_g, at

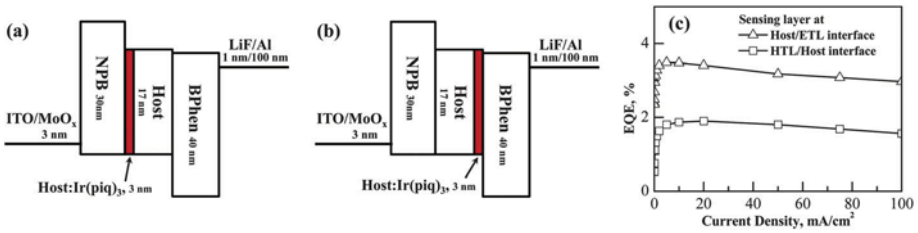

Fig. 8 Devices incorporating a sensing layer located at (a) HTL/host interface and (b) host/ETL interface, and (c) EQEs as a function of current density for the devices described in parts (a) and (b).

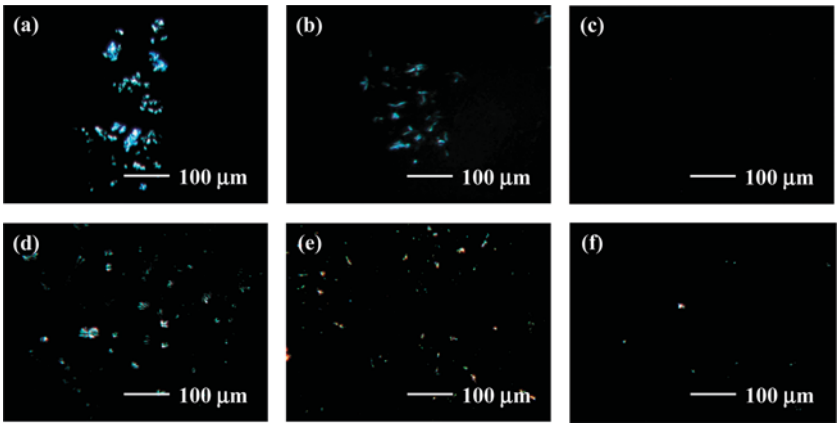

Fig. 9 Polarizing optical micrographs of 90 nm thick vacuum-sublimed, glassy films sandwiched between ITO and Al under thermal annealing at 60 °C: (a) ***t*Bu-TPA-*p*-TRZ** for 5 days; (b) ***t*Bu-TPA-*m*-TRZ** for 53 days; (c) ***t*Bu-TPA-𝒟-TRZ** for 165 days; and polarizing optical micrographs 20 nm-thick vacuum-sublimed, glassy films doped with **Ir(piq)$_3$** at a 8 wt% sandwiched between ITO and Al under thermal annealing at 75 °C: (d) ***t*Bu-TPA-*p*-TRZ:Ir(piq)$_3$** for 1 h, (e) ***t*Bu-TPA-*m*-TRZ:Ir(piq)$_3$** for 7 h, and (f) ***t*Bu-TPA-𝒟-TRZ:Ir(piq)$_3$** for 36 h.

99 and 85 °C, respectively, while ***t*Bu-TPA-*p*-TRZ** exhibits T_g at 132 °C followed by crystallization at 192 °C and then crystalline melting at 282 °C (Fig. S3a†). Thermal annealing at 60 °C of amorphous neat films of the three hybrids in ITO(100 nm)/host(90 nm)/Al(100 nm) exhibited widely varying morphological stability, five days for the ***p***-hybrid and 53 days for the ***m***-hybrid to crystallize, while the *𝒮*-hybrid showed no evidence of crystallization up to 165 days (Fig. 9a–c). Therefore, the stronger morphological stability of a glassy film does not necessarily follow from the higher T_g. As noted previously,[7] it is the conformational multiplicity rendered by the propylene spacer, rather than the high T_g, that contributes to a higher Gibbs free energy barrier to crystallization from glassy films of ***t*Bu-TPA-*𝒮*-TRZ** compared to ***t*Bu-TPA-*p*-TRZ** and ***t*Bu-TPA-*m*-TRZ**. To expedite morphological changes for experimental observation, doped films in ITO(100 nm)/host:Ir(piq)$_3$(8 wt%, 20 nm)/Al(100 nm) were thermally annealed at 75 °C, *i.e.* below respective T_gs at 135, 107, and 88 °C of EMLs consisting of ***p***-, ***m***-, and *𝒮*-hybrids (Fig. S3b†). Polycrystallinity emerged under polarizing optical microscopy with ***t*Bu-TPA-*p*-TRZ:Ir(piq)$_3$** and ***t*Bu-TPA-*m*-TRZ:Ir(piq)$_3$** in 1 and 7 h, respectively, while ***t*Bu-TPA-*𝒮*-TRZ:Ir(piq)$_3$** remained amorphous until 36 h when crystallization set in (Fig. 9d–f). The nature of microcrystallites in these doped films remains to be identified as part of the construction of phase diagrams. Nevertheless, the relative morphological stability of ***t*Bu-TPA-*𝒮*-TRZ:Ir(piq)$_3$** should contribute at least in part to the longevity of the corresponding PhOLED, as demonstrated through the correlation of device instability with thermally activated crystallization in EML.[44]

Experimental section

Materials

N,*N*′-Diphenyl-*N*,*N*′-bis(1-napthyl)-1,1′-biphenyl-4,4′-diamine (**NPB**, >99%, Kodak), 4,7-diphenyl-[1,10]phenanthroline (**BPhen**, >99%, Nichem, Taiwan), and tris(1-phenyl-isoquinolinolato-C2,N)iridium(III) (**Ir(piq)$_3$**, >99%, Kodak) were used as received without further purification. Synthesis, purification, and characterization data are described as follows for 2-(4-(4-(*N*,*N*-bis(4-(1,1-dimethylehtyl)phenyl)amino)phenyl)phenyl)-4,6-diphenyl-1,3,5-triazine, ***t*Bu-TPA-*p*-TRZ**, 2-(3-(3-(*N*,*N*-bis(4-(1,1-dimethylehtyl)phenyl)-amino)phenyl)-phenyl)-4,6-diphenyl-1,3,5-triazine, ***t*Bu-TPA-*m*-TRZ**, and 2-(4-(3-(4-(*N*,*N*-bis(4-(1,1-dimethyl-ethyl)-phenyl)amino)phenyl)propyl)phenyl)-4,6-diphenyl-1,3,5-triazine, ***t*Bu-TPA-*𝒮*-TRZ**.

Synthesis and characterization of bipolar hybrids

Synthesized according to Scheme S1,† bipolar hybrids were purified following the procedures described in the ESI.† Proton-NMR spectra in $CDCl_3$ acquired with an Avance-400 spectrometer (400 MHz) are compiled in Fig. S4–S7† for ***t*Bu-TPA-*p*-TRZ**, ***t*Bu-TPA-*m*-TRZ**, and ***t*Bu-TPA-*𝒮*-TRZ** in addition to ***t*Bu-TPA** and **TRZ**. Elemental analysis was carried out at the Elemental Analysis Facility, University of Rochester. Molecular weights were measured with a MALDI-TOF mass spectrometer (Brüker Autoflex III).

Morphology and phase transition temperatures

Thermal transition temperatures were acquired on a differential scanning calorimetry (Perkin-Elmer DSC-7) with nitrogen flow at 20 ml min^{-1}. Samples were preheated to above their melting points, and then cooled down to −30 °C at −100 °C min^{-1} before the second heating and cooling scans were recorded at 20 °C min^{-1}. All three hybrids doped with **Ir(piq)$_3$** at 8 wt% were prepared by co-dissolution in chloroform. The nature of phase transition was characterized by hot-stage polarizing optical microscopy (DMLM, Leica, FP90 central processor and FP82 hot-stage, Mettler Toledo). Film morphology was characterized by polarizing optical microscopy (Leitz Orthoplan-Pol) and recorded with a digital camera (MicroPix C-1024).

Photophysical properties

Thin films were prepared by thermal vacuum evaporation on fused silica substrates at 4 Å s^{-1} under 5 × 10^{-6} torr. The thickness was measured by a stylus-type profilometer (D-100, KLA Tencor). Absorption and photoluminescence of the resulting thin films and dilute solutions in chloroform were characterized with a UV-vis-NIR spectrophotometer (Lambda-900, Perkin-Elmer) and a spectrofluorimeter (Quanta Master C-60SE, Photon Technology International), respectively. Phosphorescence measurements were conducted for hybrids in dichloromethane at 77 K (the liquid nitrogen temperature) by a spectrofluorometer (FluoroMax-P, Horiba Jobin Yvon Inc.) equipped with a microsecond flash lamp as the pulsed excitation source. A 10 ms delay time was inserted between the pulsed excitation and the collection of the emission spectrum. The triplet energies of the compounds were determined by the highest-energy vibronic sub-bands of the phosphorescence spectra. The photoluminescence quantum yields, PLQYs, of organic thin films deposited on quartz substrates were characterized with excitation by the 325 nm line of a He–Cd laser in a calibrated integrating sphere (Labsphere Inc.) coupled to a CCD spectrograph.[45]

Electrochemical characterization

Cyclic voltammetry was conducted on an EC-Epsilon potentiostat (Bioanalytical Systems Inc.) A silver/silver chloride (Ag/AgCl) wire, a platinum wire, and a glassy carbon disk with a 3 mm diameter were used as the reference, counter, and working electrodes, respectively. Tetraethylammonium tetrafluoroborate was used as the supporting electrolyte, which had been purified as described previously.[46] Samples were dissolved at a concentration of 10^{-3} M in acetonitrile/toluene (1 : 1 by volume) containing 0.1 M supporting electrolyte. Acetonitrile and toluene were distilled with calcium hydride and sodium/benzophenone, respectively. The dilute sample solutions exhibit reduction and oxidation scans against the Ag/AgCl reference electrode. The reduction and oxidation potentials were adjusted to ferrocene (Fc) as an internal standard with an oxidation potential of 0.51 ± 0.02 V with respect to Ag/AgCl. The reduction and oxidation potentials, $E_{1/2}$(red) and $E_{1/2}$(oxd), relative to (Fc/Fc$^+$) were used to calculate the LUMO and HOMO

levels as $-4.80 - qE_{1/2}$(red) eV and $-4.80 - qE_{1/2}$(oxd) eV, respectively, where q is electron charge.[47]

PhOLED and unipolar device fabrication and characterization

ITO substrates were thoroughly cleaned and treated with oxygen plasma prior to depositing a 3 nm-thick MoO_x layer by thermal vacuum evaporation at 0.3 Å s^{-1}, followed by a hole-transport layer (30 nm), NPB, and an EML (20 nm) comprising host:Ir(piq)$_3$ at a mass ratio of 8%, both at 4 Å s^{-1}. Layers of BPhen (40 nm) and LiF (1 nm) were consecutively deposited at 4 Å s^{-1} and 0.2 Å s^{-1}, respectively. The devices were completed by deposition of aluminum (100 nm) at 10 Å s^{-1} through a shadow mask to define an active area of 0.1 cm^2. All evaporation processes were carried out at a base pressure less than 5×10^{-6} torr. The unipolar devices and PhOLEDs containing the sensing [**Ir(piq)$_3$** containing] layer were fabricated by the same procedure. All PhOLEDs were characterized by a source-measure unit (Keithley 2400) and a spectroradiometer (PhotoResearch PR650) in the ambient environment without encapsulation. The front-view performance data were collected, and the EQEs were calculated assuming the Lambertian distribution of emission intensities. The current–voltage characterizations of the unipolar devices were carried out using a source-measure unit (Keithley 2400).

Summary

Three representative bipolar hybrid compounds with distinct chemical linkages, ***t*Bu-TPA-*p*-TRZ**, ***t*Bu-TPA-*m*-TRZ**, and ***t*Bu-TPA-𝒮-TRZ**, were synthesized to evaluate their potential as hosts for PhOLEDs. Mediated by intramolecular and intermolecular processes, the CTC formation in all three hybrids was diagnosed with fluorescence bathochromism at an increasing solvent polarity. The ***p***-hybrid is by far the most susceptible to CTC formation, while the 𝒮-hybrid is the least. The E_T values decrease from ***t*Bu-TPA-𝒮-TRZ** (3.0 eV) through the ***m***- (2.7 eV) to the ***p***-hybrid (2.5 eV), all suitable for hosting red-emitting **Ir(piq)$_3$**, but the ***m***- and ***p***-hybrids would not be viable for blue-emitting **FIrpic**. The three hybrids were tested in red-emitting PhOLEDs to elucidate the effects of CTC formation and relative balance between charge fluxes as assessed by hole-only, electron-only, and sensing-layer-containing PhOLED devices. The lowest external quantum yield was encountered with ***t*Bu-TPA-*p*-TRZ** because of the most extensive CTC formation overshadowing the best balanced charge fluxes. The superior EQE and lower driving voltage of ***t*Bu-TPA-*m*-TRZ** over ***t*Bu-TPA-𝒮-TRZ** are attributed to the better balanced charge fluxes using ***t*Bu-TPA-*m*-TRZ** despite the lesser extent of CTC formation using ***t*Bu-TPA-𝒮-TRZ**. The least CTC formation in the 𝒮-hybrid allows accommodation of the most singlets and triplets following charge recombination. Because of its higher E_T value than those of **Ir(piq)$_3$** and **FIrpic**, energy transfer is favorable to enhancing EQE of the resulting PhOLEDs. Additionally, the flexible linkage in ***t*Bu-TPA-𝒮-TRZ** has been demonstrated to produce the desired glassy EML with the best morphological stability. Beyond the scope of this work, it should be noted that the modest EQEs reported herein can be significantly improved by optimizing several parameters, *e.g.* aligning the energy levels between neighboring layers, minimizing charge accumulation at interfaces, balancing charge fluxes, and distributing excitons evenly across EML through engineering of chemical composition and device architecture. The results from this continuing effort will be reported in due course.

Acknowledgements

Qiang Wang, Jason U. Wallace, Thomas Y.-H. Lee, and Shaw H. Chen thank Professor Ching W. Tang, Dr Lichang Zeng, and Mr Kevin P. Klubek for their technical advice and helpful discussions, and especially to Professor Ching W. Tang for access to the PhOLED device fabrication and characterization facilities. They acknowledge the financial support by the Department of Energy under Grant no. DE-EE0003296 for a solid-state lighting team project. Additional funding was provided by the Department of Energy Office of Inertial Confinement Fusion under Cooperative Agreement no. DE-FC52-08NA28302 with Laboratory for Laser Energetics at the University of Rochester. The support of DOE does not constitute an endorsement by DOE of the views expressed in this article. In addition, Yu-Tang Tsai, Yi-Hsiang Huang, and Chung-Chih Wu are grateful for the financial support by the National Science Council (Grant NSC-99-2221-E-002-118-MY3) and Ministry of Education (Grant 10R70607-2) of Taiwan.

References

1 L. Xiao, Z. Chen, B. Qu, J. Luo, S. Kong, Q. Gong and J. Kido, *Adv. Mater.*, 2011, **23**, 926.
2 M. A. Baldo, S. Lamansky, P. E. Burrows, M. E. Thompson and S. R. Forrest, *Appl. Phys. Lett.*, 1999, **75**, 4.
3 T. K. Hatwar, M. E. Kondakova, D. J. Giesen and J. P. Spindler, in *Organic Electronics: Materials, Processing, Devices and Applications*, ed. F. So, CRC Press, Boca Raton, 2010, pp. 468–488.
4 Y. Tao, C. Yang and J. Qin, *Chem. Soc. Rev.*, 2011, **40**, 2943.
5 Z. Ge, T. Hayakawa, S. Ando, M. Ueda, T. Akiike, H. Miyamoto, T. Kajita and M. Kakimoto, *Chem. Mater.*, 2008, **20**, 2532.
6 Y. Tao, Q. Wang, C. Yang, C. Zhong, K. Zhang, J. Qin and D. Ma, *Adv. Funct. Mater.*, 2010, **20**, 304.
7 L. Zeng, T. Y.-H. Lee, P. B. Merkel and S. H. Chen, *J. Mater. Chem.*, 2009, **19**, 8772.
8 S. Gong, Y. Chen, J. Luo, C. Yang, C. Zhong, J. Qin and D. Ma, *Adv. Funct. Mater.*, 2011, **21**, 1168.
9 C.-H. Chen, W.-S. Huang, M.-Y. Lai, W.-C. Tsao, J. T. Lin, Y.-H. Wu, T.-H. Ke, L.-Y. Chen and C.-C. Wu, *Adv. Funct. Mater.*, 2009, **19**, 2661.
10 T. Förster, in *The Exciplex*, ed. M. Gordon and W. R. Ware, Academic Press, New York, 1975, ch. 1.
11 N. Matsumoto, M. Nishiyama and C. Adachi, *J. Phys. Chem. C*, 2008, **112**, 7735.
12 Y. Hino, H. Kajii and Y. Ohmori, *Jpn. J. Appl. Phys., Part 1*, 2005, **44**, 2790.

13 H.-F. Chen, S.-J. Yang, Z.-H. Tsai, W.-Y. Hung, T.-C. Wang and K.-T. Wong, *J. Mater. Chem.*, 2009, **19**, 8112.
14 M. M. Rothmann, S. Haneder, E. Da Como, C. Lennartz, C. Schildknecht and P. Strohriegl, *Chem. Mater.*, 2010, **22**, 2403.
15 E. Polikarpov, J. S. Swensen, N. Chopra, F. So and A. Padmaperuma, *Appl. Phys. Lett.*, 2009, **94**, 223304.
16 Y. Tao, Q. Wang, Y. Shang, C. Yang, L. Ao, J. Qin, D. Ma and Z. Shuai, *Chem. Commun.*, 2009, 77.
17 E. T. Seo, R. F. Nelson, J. M. Fritsch, L. S. Marcoux, D. W. Leedy and R. N. Adams, *J. Am. Chem. Soc.*, 1966, **88**, 3498.
18 R. Fink, Y. Heischkel, M. Thelakkat, H.-W. Schmidt, C. Jonda and M. Hüppauff, *Chem. Mater.*, 1998, **10**, 3620.
19 W. L. Jia, X. D. Feng, D. R. Bai, Z. H. Lu, S. Wang and G. Vamvounis, *Chem. Mater.*, 2005, **17**, 164.
20 T.-H. Huang, J. T. Lin, L.-Y. Chen, Y.-T. Lin and C.-C. Wu, *Adv. Mater.*, 2006, **18**, 602.
21 Z. R. Grabowski and K. Rotkiewicz, *Chem. Rev.*, 2003, **103**, 3899.
22 H. Beens and A. Weller, in *Organic Molecular Photophysics*, ed. J. B. Birks, Wiley, London, 1975, vol. 2, pp. 159–163.
23 S.-J. Su, H. Sasabe, Y.-J. Pu, K.-i. Nakayama and J. Kido, *Adv. Mater.*, 2010, **22**, 3311.
24 S. Y. Lee, *Bull. Korean Chem. Soc.*, 1998, **19**, 93.
25 H.-S. Im and E. R. Bernsteinm, *J. Chem. Phys.*, 1988, **88**, 7337.
26 G. V. Loukova, D. K. Susarova and V. A. Smirnov, *Russ. Chem. Bull.*, 2008, **57**, 257.
27 B. W. D'Andrade, D. Datta, S. R. Forrest, P. Djurovich, E. Polikarpov and M. E. Thompson, *Org. Electron.*, 2005, **6**, 11.
28 P. I. Djurovich, E. I. Mayo, S. R. Forrest and M. E. Thompson, *Org. Electron.*, 2009, **10**, 515.
29 A. Weller, *Pure Appl. Chem.*, 1968, **16**, 115.
30 A. Tsuboyama, H. Iwawaki, M. Furugori, T. Mukaide, J. Kamatani, S. Igawa, T. Moriyama, S. Miura, T. Takiguchi, S. Okada, M. Hoshino and K. Ueno, *J. Am. Chem. Soc.*, 2003, **125**, 12971.
31 M. A. Baldo, C. Adachi and S. R. Forrest, *Phys. Rev. B: Condens. Matter*, 2000, **62**, 10967.
32 D. Song, S. Zhao, Y. Luo and H. Aziz, *Appl. Phys. Lett.*, 2010, **97**, 243304.
33 S. E. Shaheen, G. E. Jabbour, M. M. Morrel, Y. Kawabe, B. Kippelen, N. Peyghambarian, M.-F. Nabor, R. Schlaf, E. A. Mash and N. R. Armstrong, *J. Appl. Phys.*, 1998, **84**, 2324.
34 B. Liang, C. Jiang, Z. Chen, X. Zhang, H. Shi and Y. Cao, *J. Mater. Chem.*, 2006, **16**, 1281.
35 F. Wang, X. Qiao, T. Xiong and D. Ma, *Org. Electron.*, 2008, **9**, 985.
36 J. Meyer, M. Kröger, S. Hamwi, F. Gnam, T. Riedl, W. Kowalsky and A. Kahn, *Appl. Phys. Lett.*, 2010, **96**, 193302.
37 H.-J. Egelhaaf, J. Gierschner and D. Oelkrug, *Synth. Met.*, 2002, **127**, 221.
38 B. P. Lyons, K. S. Wong and A. P. Monkman, *J. Chem. Phys.*, 2003, **118**, 4707.
39 C. Adachi, R. C. Kwong, P. Djurovich, V. Adamovich, M. A. Baldo, M. E. Thompson and S. R. Forrest, *Appl. Phys. Lett.*, 2001, **79**, 2082.
40 E. Holder, B. M. W. Langeveld and U. S. Schubert, *Adv. Mater.*, 2005, **17**, 1109.
41 M. Castellani and D. Berner, *J. Appl. Phys.*, 2007, **102**, 024509.
42 C. W. Tang, S. A. VanSlyke and C. H. Chen, *J. Appl. Phys.*, 1989, **85**, 3610.
43 R. Meerheim, S. Scholz, S. Olthof, G. Schwartz, S. Reineke, K. Walzer and K. Leo, *J. Appl. Phys.*, 2008, **104**, 014510.
44 T. Y.-H. Lee, Q. Wang, J. U. Wallace and S. H. Chen, *J. Mater. Chem.*, 2012, **22**, 23175.
45 Y. Kawamura, H. Sasabe and C. Adachi, *Jpn. J. Appl. Phys., Part 1*, 2004, **43**, 7729.
46 L. Zeng, F. Yan, S. K.-H. Wei, S. W. Culligan and S. H. Chen, *Adv. Funct. Mater.*, 2009, **19**, 1978.
47 J. Pommerehne, H. Vestweber, W. Guss, R. F. Mahrt, H. Bässler, M. Porsch and J. Daub, *Adv. Mater.*, 1995, **7**, 551.

